

GASEOUS MATERIAL ORBITING THE POLLUTED, DUSTY WHITE DWARF HE 1349–2305

CARL MELIS^{1,8}, P. DUFOUR², J. FARIHI³, J. BOCHANSKI⁴, ADAM J. BURGASSER^{1,4}, S. G. PARSONS⁵, B. T. GÄNSICKE⁵,
D. KOESTER⁶, AND BRANDON J. SWIFT⁷

¹ Center for Astrophysics and Space Sciences, University of California, San Diego, CA 92093-0424, USA; cmelis@ucsd.edu

² Département de Physique, Université de Montréal, Montréal, QC H3C 3J7, Canada

³ Department of Physics and Astronomy, University of Leicester, Leicester LE1 7RH, UK

⁴ Massachusetts Institute of Technology, Kavli Institute for Astrophysics and Space Research, Building 37, Room 664B,
77 Massachusetts Avenue, Cambridge, MA 02139, USA

⁵ Department of Physics, University of Warwick, Coventry CV4 7AL, UK

⁶ Institut für Theoretische Physik und Astrophysik, University of Kiel, 24098 Kiel, Germany

⁷ Steward Observatory, University of Arizona, 933 North Cherry Avenue, Tucson, AZ 85721, USA

Received 2012 March 2; accepted 2012 April 3; published 2012 April 30

ABSTRACT

We present new spectroscopic observations of the polluted, dusty, helium-dominated atmosphere white dwarf star HE 1349–2305. Optical spectroscopy reveals weak Ca II infrared triplet emission indicating that metallic gas debris orbits and is accreted by the white dwarf. Atmospheric abundances are measured for magnesium and silicon while upper limits for iron and oxygen are derived from the available optical spectroscopy. HE 1349–2305 is the first gas disk-hosting white dwarf star identified among previously known polluted white dwarfs. Further characterization of the parent body polluting this star will require ultraviolet spectroscopy.

Key words: circumstellar matter – planet–star interactions – stars: abundances – stars: individual (HE 1349–2305) – white dwarfs

Online-only material: color figure

1. INTRODUCTION

White dwarf stars are now known to be polluted by remnant rocky bodies from planetary systems that otherwise stably orbited their host star while it was on the main sequence (e.g., Zuckerman et al. 2007, 2010; Jura 2008; Farihi et al. 2009, 2010a, 2010b; Dufour et al. 2010; Klein et al. 2010, 2011; Melis et al. 2010, and references therein). Prior to being accreted, these rocky bodies are tidally shredded into disks of dusty material (e.g., Debes & Sigurdsson 2002; Jura 2003). A subset of dusty white dwarfs also host disks of gaseous metals which similarly have their origin in the disintegration of remnant rocky bodies from the white dwarf planetary system (Gänsicke et al. 2006, 2007, 2008a; Melis et al. 2010; Farihi et al. 2011b; Brinkworth et al. 2012).

Koester et al. (2005) and Voss et al. (2007) describe the atmospheric properties of the DBAZ (helium-dominated atmosphere with hydrogen and heavy-element pollution) white dwarf star HE 1349–2305 (J2000 R.A. and decl. of 13 52 44.12 and –23 20 05.3; Epchtein et al. 1997). Girven et al. (2012) detect excess infrared emission toward HE 1349–2305 indicating that it hosts and accretes from a dusty circumstellar disk. As a result of parallels between this source and the potentially water-rich object GD 61 (Farihi et al. 2011a; Jura & Xu 2012), we obtained spectroscopic data for HE 1349–2305 to constrain its heavy-element abundances and oxygen content. An unexpected discovery in these spectroscopic data was the detection of emission lines indicating the presence of an orbiting gaseous disk. Here we describe observations of HE 1349–2305 and place it in the context of other gas disk-hosting white dwarfs.

2. OBSERVATIONS

2.1. Nickel Optical Imaging

Optical imaging was performed on UT 2010 March 24 at Lick Observatory with the 40 inch Nickel telescope. These observations used the facility’s Direct Imaging Camera (CCD-C2), a 2048 × 2048 pixel detector with 15 μm pixels. The 0′.184 pixel^{−1} plate scale affords a field of view of roughly 6′.3 squared. The detector was binned by two in rows and columns and was readout in fast mode.

HE 1349–2305 was observed in the V band (Bessell 1990). A four-step dither pattern with 10′ steps was repeated with 60 s integrations per step position. Similar observations were performed for the flux calibrator source Gl 529 (Bessel 1990). Images are reduced by median-combining all frames to obtain a sky frame and subtracting this sky frame from each image. Sky-subtracted images are then divided by flat-field frames obtained by imaging the twilight sky. Each science frame is registered using bright stars in the field and then all science frames are median combined to yield the final reduced image. Detector counts for HE 1349–2305 and Gl 529 are extracted with an aperture that yields ≈85% encircled energy (with a negligible correction between the two sources). This is achieved by extracting counts for both stars with a 4 binned-pixel (1′.5) radius circular aperture. The sky is sampled with an annulus extending from 20 to 60 pixels. Uncertainties are derived from the dispersion of measurements made from individually reduced frames. The uncertainties for Gl 529 are propagated into the final quoted uncertainty for HE 1349–2305.

Nickel photometry is reported in Table 1 which also includes the DENIS (Epchtein et al. 1997) I band magnitude and *Galaxy Evolution Explorer* (GALEX; Martin et al. 2005) fluxes.

2.2. Gemini Imaging at the Shane 3 m

Observations of HE 1349–2305 in the *J*, *H*, and *K′* bands were performed UT 2010 March 28 with the Gemini

⁸ Joint CASS Departmental Fellow and NSF AAPF Fellow.

Table 1
Broadband Fluxes for HE 1349–2305

Band	λ (nm)	m (mag)	F_{obs} (mJy)
Lick-Gemini camera—NIR			
<i>H</i>	1650	16.87 ± 0.08	0.19 ± 0.01
<i>J</i>	1240	16.85 ± 0.06	0.30 ± 0.02
DENIS—infrared			
<i>I</i>	798.2	16.70 ± 0.09	0.50 ± 0.04
Nickel 40 inch—optical			
<i>V</i>	544.8	16.22 ± 0.11	1.17 ± 0.12
<i>GALEX</i> —ultraviolet			
NUV	227.1	16.24 ± 0.03	1.16 ± 0.04
FUV	152.8	16.54 ± 0.08	0.88 ± 0.06

Note. Gemini, DENIS (Epchtein et al. 1997), and Nickel magnitudes are on the Vega system. *GALEX* measurements are in AB magnitudes. The *GALEX* NUV uncertainty is as suggested in Morrissey et al. (2007) while the FUV uncertainty is representative of the scatter between the two separate *GALEX* detections of HE 1349–2305.

Twin-Arrays Infrared Camera (McLean et al. 1993) mounted on the 3 m Shane telescope at Lick Observatory. We used a four position dither pattern with exposure times of 10, 5, and 7 s with co-adds of 15, 30, and 21 per position for each of *JHK'*, respectively. Total on source integration times of 1800 s were accrued at each of *JH* while 3528 s were obtained for *K'*. The $\approx 3'$ field of view of the Gemini instrument enabled simultaneous observations of two Two Micron All Sky Survey (Skrutskie et al. 2006) sources for use in flux calibration.

Data are reduced using in-house IDL software routines. For each filter, science frames are median combined to generate a sky-median frame which is then subtracted from each science frame. Sky-subtracted frames are then flat fielded using exposures of the twilight sky for *JK'* and the illuminated telescope dome for *H*. Reduced science frames are registered with bright point sources within the field. Although data were recorded for the longer wavelength chip (*K'*), they are not usable for accurate photometric measurements due to instrumental difficulties. The Gemini photometric results for HE 1349–2305 are reported in Table 1. *JH* band results presented herein are consistent with those presented by Girven et al. (2012).

2.3. MagE Optical Spectroscopy

Moderate resolution optical spectroscopy of HE 1349–2305 was obtained on UT 2011 March 19 with the Magellan Echellette (MagE; Marshall et al. 2008) mounted on the 6.5 m Landon Clay Telescope at Las Campanas Observatory. One 900 s exposure was obtained with the 0'.5 slit aligned with the parallactic angle; this setup provided 3200–10050 Å spectroscopy with a resolving power of $\approx 11,000$.

Data are reduced using the MASE reduction pipeline (Bochanski et al. 2009) following standard procedures for order tracing, flat-field correction, wavelength calibration (with ThAr lamp spectra), heliocentric wavelength correction, optimal source extraction, order stitching, and flux calibration via observations of Hiltner 600 (Hamuy et al. 1994).

2.4. SpeX Near-infrared Spectroscopy

Near-infrared spectroscopy was obtained with SpeX (Rayner et al. 2003) mounted on the 3 m NASA IRTF telescope

on UT 2011 April 22. Prism-mode observations covering 0.8–2.5 μm were performed with a 0'.8 slit aligned with the parallactic angle. Six ABBA nod patterns were obtained for HE 1349–2305 with 60 s of integration time and two co-adds per nod position. A single AB nod pair of 0.51 s integration time and 10 co-adds per nod position was obtained for the telluric calibration source HD 119752 (A0 V). Data are reduced with SpeXTool (Cushing et al. 2004; Vacca et al. 2003). Absolute flux calibration of the HE 1349–2305 prism data is accomplished by scaling its spectrum to the Gemini *JH*-band measurements.

It is noted that the SpeX data smoothly connect all available near-infrared photometric data for HE 1349–2305 (Table 1 and Girven et al. 2012).

2.5. VLT X-shooter Spectroscopy

Moderate resolution spectroscopy of HE 1349–2305 was obtained in service mode with X-shooter (D'Odorico et al. 2006) mounted on the 8.2 m VLT UT2 (Kueyen) telescope. One observation was obtained on UT 2011 May 26 while two more were obtained on UT 2011 May 28. UVB arm (3000–5600 Å) observations were performed with the 0'.5 slit resulting in a resolving power of 9,900 and exposed for 1475 s per observation. VIS arm (5500–10200 Å) observations were performed with the 0'.4 slit resulting in a resolving power of 18,200 and exposed for 1420 s per observation. Raw frames are reduced using the X-shooter pipeline version 1.3.7 within ESOREX.⁹ Standard X-shooter data reduction techniques are employed with default settings to extract and wavelength calibrate each spectrum. Relative flux calibration on the science spectrum is performed with the use of the spectrophotometric standards LTT 3218 (May 26th) and EG 274 (May 28th) to derive the instrumental response function. Although X-shooter coverage extends to the thermal infrared, data beyond $\approx 1 \mu\text{m}$ are unusable due to low recorded signal.

3. RESULTS AND MODELING

Physical parameters for HE 1349–2305 are adopted from analysis performed on VLT UVES spectra in Koester et al. (2005) and Voss et al. (2007); namely, T_{eff} of 18,173 K, $\log g$ of 8.13 (cgs units), and a mass of $0.673 M_{\odot}$. By matching a model white dwarf atmosphere with these parameters to the observed spectra and photometry we derive a distance to the white dwarf of 120 ± 10 pc (the uncertainty here does not take into account uncertainties on the white dwarf parameters). Spectral observations that extend to wavelengths of $\approx 2.5 \mu\text{m}$ confirm the results of Girven et al. (2012), but are not capable of further restricting the dusty disk parameters. From absorption lines detected in the optical spectra we derive observed radial velocities (which include contributions from gravitational redshift and stellar motion) of 40 ± 30 and $40 \pm 5 \text{ km s}^{-1}$ from the MagE and UVES data, respectively. Difficulties in setting the wavelength zero-point in the X-shooter data prevent any meaningful radial velocity measurement—these data are corrected to the white dwarf reference frame by assuming the radial velocity is the same as that measured for the MagE and UVES data. The contribution from gravitational redshift is estimated to be 35 km s^{-1} and hence the white dwarf systemic motion is $\sim 5 \text{ km s}^{-1}$.

⁹ The ESO Recipe Execution Tool: <http://www.eso.org/sci/software/cpl/esorex.html>; version 3.9.0 is used.

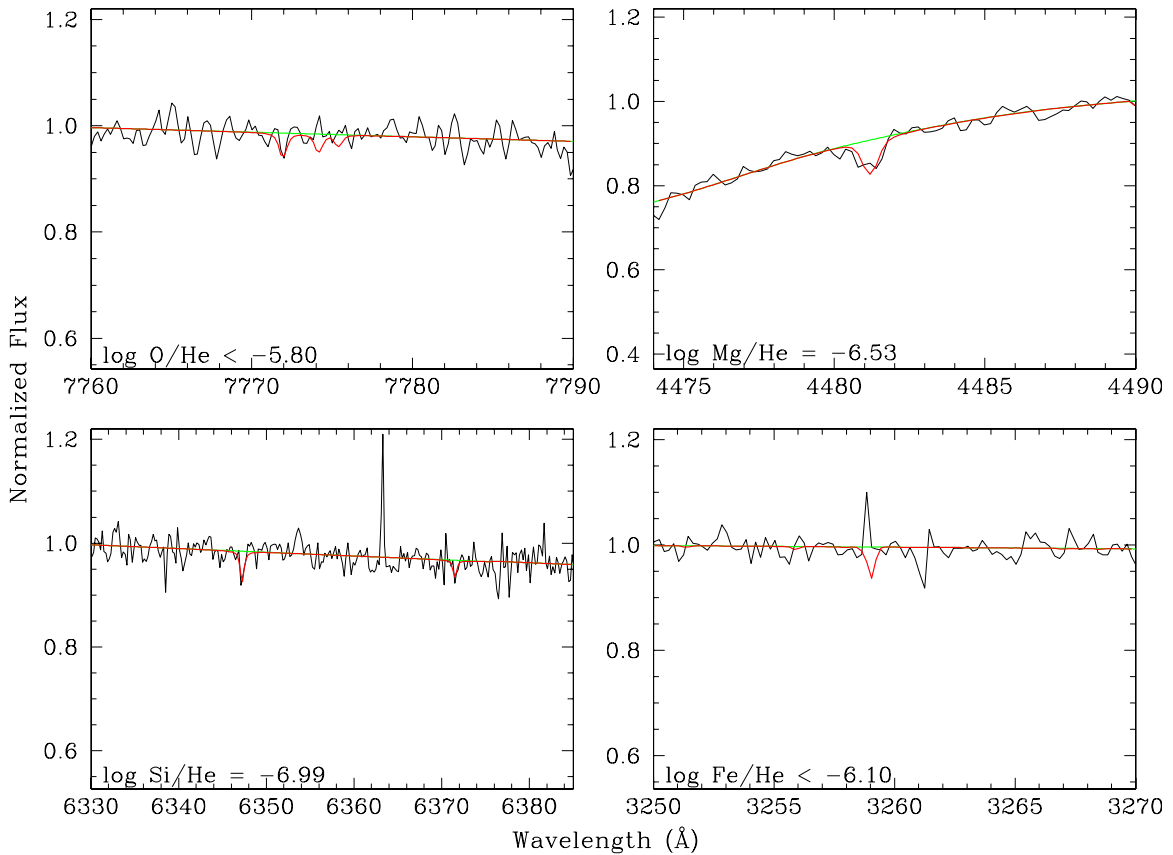


Figure 1. New abundances and limits from the X-shooter spectra of HE 1349–2305. The emission spikes in the spectra are from cosmic rays. Magnesium is well detected, silicon is detected, and iron and oxygen are not detected. The limits reported in the panels for oxygen and iron correspond to the absorption line strengths shown in their respective panels; the adopted upper limits listed in Table 2 are for slightly stronger lines which would have been well detected in the spectrum if they were present. The black curve is the data, the red overplotted curve is the model, and the green overplotted curve is the model with the element of interest removed. Wavelengths in this figure are presented in air.

(A color version of this figure is available in the online journal.)

3.1. Abundances

No absorption lines other than those from H I and He I are significantly detected in the MagE spectrum (Ca II H and K lines are marginally detected, but not useful for abundance modeling). The X-shooter data enable the additional detection of Mg II, Si II (Figure 1), and Ca II. Koester et al. (2005) and Voss et al. (2007) report detections of H I and Ca II in their UVES spectra. To try and explore the water content of the body polluting HE 1349–2305 we calculated upper limits for the abundances of oxygen and iron, the two major constituents of terrestrial rocky minerals not detected (Figure 1). We use a local thermodynamic equilibrium model atmosphere code similar to that described in Dufour et al. (2005, 2007). Absorption line data are taken from the Vienna Atomic Line Database.¹⁰ We calculate grids of synthetic spectra for each element of interest. The grids cover a range of abundances typically from $\log[n(Z)/n(\text{He})] = -3.0$ to -7.0 in steps of 0.5 dex. We determine abundances or limits by fitting the expected position of various lines in the spectra using a similar method to that described in Dufour et al. (2005). Briefly, this is done by minimizing the value of χ^2 which is taken to be the sum of the difference between the normalized observed and model fluxes over the frequency range of interest with all frequency points being given an equal weight. Upper limits are derived by comparing model lines of a given abundance with

their expected position in the spectra and determining whether such a line would be detectable given the local signal-to-noise ratio of the spectrum.

All abundance measurements for HE 1349–2305 are reported in Table 2. Abundance measurements for hydrogen and calcium agree within the errors with those reported in Koester et al. (2005) and Voss et al. (2007).

3.2. Gas Emission Lines

Broad emission lines from the Ca II infrared triplet (IRT) are detected in the MagE and X-shooter spectra (Figure 2). For each feature we measure the maximum gas velocity in the blue and red wings of the detected emission lines, full velocity width at zero power, and the line flux; these values are reported in Table 3. It is not possible to place robust constraints on the gas disk inner and outer radii with the available spectra. Modeling similar to that described in Gänsicke et al. (2006) suggests that the gas disk outer radius is similar to those of the other gas disk-hosting white dwarf stars, $\sim 100 R_{\text{WD}}$. From the maximum velocity gas seen in the disk, and assuming a disk inclination angle of 60° (in accordance with inclination angle values used in modeling of white dwarf dust disks—see, e.g., Farihi et al. 2009), we estimate a disk inner radius of $\sim 15 R_{\text{WD}}$. If we employ the inclination angle derived by Girven et al. (2012) for the dust disk orbiting HE 1349–2305— $i \approx 85^\circ$ —then the inner radius of the gas disk is slightly higher at $\sim 20 R_{\text{WD}}$.

¹⁰ <http://vald.astro.univie.ac.at/~vald/php/vald.php>

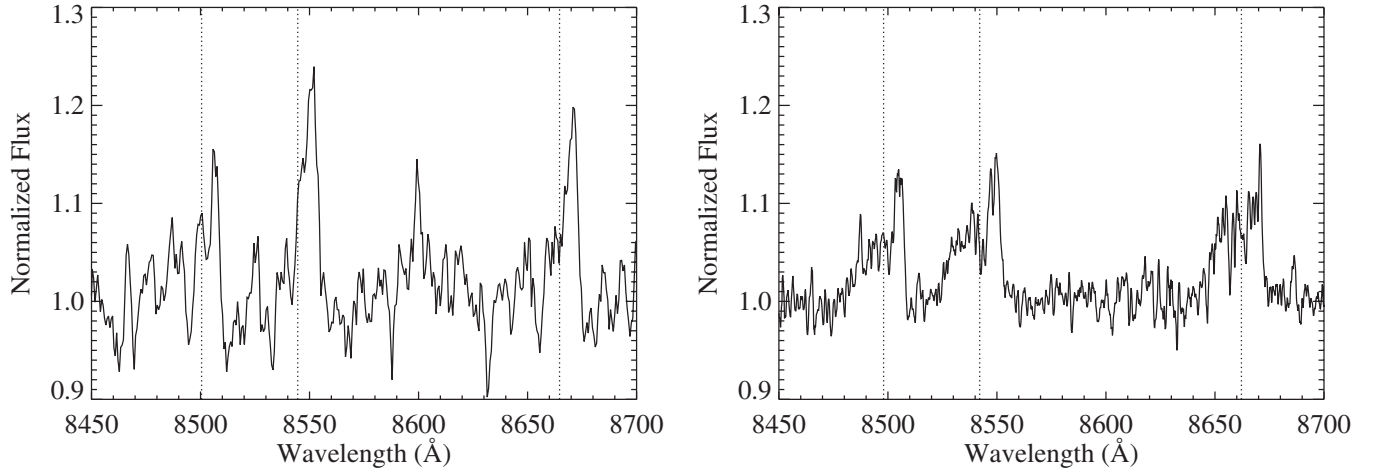


Figure 2. Gas disk emission lines in the MagE (left) and X-shooter (right) spectra of HE 1349–2305. The MagE data have been smoothed with a 5 pixel boxcar—the low signal-to-noise ratio likely prevents detection of the weaker emission hump evident in the X-shooter data. The vertical dotted lines mark the estimated wavelength position of the white dwarf systemic motion (see Section 3). Wavelengths in these figures are corrected to the heliocentric reference frame and are presented in vacuum for the MagE spectrum and air for the X-shooter spectrum.

Table 2
Atmospheric Pollution of Gas Disk-hosting White Dwarfs

Star	[H/He] ^a	[O/H(e)]	[Mg/H(e)]	[Si/H(e)]	[Ca/H(e)]	[Fe/H(e)]	$\dot{M}_{\text{acc,Mg}}^{\text{b}}$	Ref.
(Logarithmic Abundances by Number)							(10^8 g s^{-1})	
HE 1349–2305	-4.9 ± 0.2	< -5.6	-6.5 ± 0.2	-7.0 ± 0.2	-7.4 ± 0.2	< -5.9	1.3	1,2,3
SDSS J0738	-5.73 ± 0.17	-3.81 ± 0.19	-4.68 ± 0.07	-4.90 ± 0.16	-6.23 ± 0.15	-4.98 ± 0.09	146.4	4,5
SDSS J0959	–	–	–5.2	–	–7.0	–	0.32	6
Ton 345	< -4.5	–	-5.2 ± 0.2	-5.1 ± 0.2	-6.9 ± 0.2	–	18.3	7
SDSS J1043	–	–	-4.94 ± 0.24	–	–	–	0.73	8
SDSS J1228	–	–	-4.58 ± 0.06	–	-5.76 ± 0.08	–	2.2	9,10

Notes.

^a Hydrogen pollution for helium-dominated atmosphere (DB) white dwarfs. A “–” in this column indicates that the star has a hydrogen-dominated atmosphere (DA) and that each elemental abundance listed is relative to hydrogen by number. In other columns a “–” indicates that no measurement exists in the literature.

^b $\dot{M}_{\text{acc,Mg}} = M_{\text{env,Mg}}/\tau_{\text{diff,Mg}}$, where $M_{\text{env,Mg}}$ is the mass of magnesium in each star’s envelope and $\tau_{\text{diff,Mg}}$ is the diffusion constant for magnesium (see Koester 2009). For helium-dominated atmosphere white dwarfs this quantity is averaged over the $\sim 10^5$ yr settling times.

References. (1) Koester et al. 2005; (2) Voss et al. 2007; (3) This work; (4) Dufour et al. 2010; (5) Dufour et al. 2012; (6) Farihi et al. 2011b; (7) Gänsicke et al. 2008a; (8) Gänsicke et al. 2007; (9) Gänsicke et al. 2006; (10) Gänsicke et al. 2008b.

Table 3
HE 1349–2305 Emission Line Measurements

Transition	Equivalent Width ^a (Å)	$v_{\text{max}} \sin i^{\text{b}}$ (km s^{-1})	Full Width ^b (km s^{-1})	Total Line Flux ^c ($10^{-15} \text{ erg cm}^{-2} \text{ s}^{-1}$)
MagE—2011 March 19				
Ca II λ 8498	1.4 ± 0.3	$-190 \pm 140/+410 \pm 110$	600 ± 180	0.30
Ca II λ 8542	2.1 ± 0.3	$-160 \pm 140/+510 \pm 140$	670 ± 200	0.45
Ca II λ 8662	1.7 ± 0.4	$-220 \pm 140/+400 \pm 70$	620 ± 160	0.37
X-shooter—average of 2011 May 26 and 28				
Ca II λ 8498	1.9 ± 0.2	$-780 \pm 110/+380 \pm 35$	1160 ± 120	0.41
Ca II λ 8542	1.7 ± 0.2	$-710 \pm 70/+450 \pm 70$	1160 ± 100	0.37
Ca II λ 8662	1.6 ± 0.3	$-740 \pm 110/+400 \pm 70$	1140 ± 130	0.35

Notes.

^a Equivalent widths are not corrected for line absorption.

^b The two different values reported for $v_{\text{max}} \sin i$ correspond to the maximum velocity gas seen in the blue and red wings of the double-peaked emission features, respectively. The blue wing is measured at the continuum blueward of the line while the red wing is measured at the continuum redward of the line. Full velocity width of the emission feature is the velocity extent from the blue to the red wings.

^c These values are computed by multiplying the reported emission line equivalent width measurements by the stellar continuum flux (as deduced from the SpeX spectrum) at the emission line location.

More precise constraints on the gas disk structure will require higher signal-to-noise ratio observations. These observations are likely better carried out using lower resolution optical spectrographs than those used herein.

4. DISCUSSION

HE 1349–2305 is found to host Ca II IRT emission lines. The lack of hydrogen or helium emission lines in the optical and infrared spectra suggests that this material is metal-rich. Material orbiting the star would be expected to exhibit a double-peaked emission line morphology similar to that seen for the other gas disk-hosting white dwarfs (Gänsicke et al. 2006, 2007, 2008a; Melis et al. 2010). Although only a single peak of emission is significantly detected in the MagE data, a weaker second peak is evident in the X-shooter data securing the Keplerian origin of the gas emission. No significant radial velocity shift is evident between the various epochs of optical spectroscopy, making the origin of the emission lines from a binary companion (or interactions therewith) unlikely. As a result, we interpret these emission lines as emanating from a gaseous debris disk similar to that described by Gänsicke et al. (2006). Support of such an interpretation is found through similarities observed for other such sources (Brinkworth et al. 2009; Melis et al. 2010) and the detection of thermal infrared excess emission toward HE 1349–2305 indicating that a dusty debris disk also orbits the star (Girven et al. 2012). The asymmetry of the emission line peak intensities is curious (Figure 2). Similar peak intensity contrast is evident at a slightly weaker level for SDSS J1228 (Gänsicke et al. 2006; Melis et al. 2010) and at a slightly stronger level in the 2004 epoch spectrum of Ton 345 (Gänsicke et al. 2008a). In regards to the sharp cutoff in line intensity on one edge of the emission complex and the slower roll-off in intensity at the other edge, the emission structure of this source resembles those of the other gas disk white dwarfs studied at high spectral resolution (Melis et al. 2010). The rough gas disk inner and outer radii are reminiscent of those measured for the other gas disk-hosting white dwarfs (Gänsicke et al. 2006, 2007, 2008a; Melis et al. 2010). The outer disk radius is consistent with the location of the Roche limit for HE 1349–2305, suggesting that its orbiting gas disk is generated by rocky objects that impinge on a pre-existing dusty debris disk (e.g., Jura 2008; Melis et al. 2010). This is further supported by the fact that the gas disk inner and outer radii are roughly consistent with the dust disk inner and outer radii reported in Girven et al. (2012). Thus, despite the inexact characterization of the structure of its orbiting gas disk, it can be concluded that HE 1349–2305 is being polluted by rocky objects from its planetary system similar to other gas disk-hosting white dwarf stars (e.g., Melis et al. 2010 and references therein).

An attempt to constrain the composition of the body polluting this star is made by examining the abundances of the major elemental constituents of rocky minerals: magnesium, silicon, iron, and oxygen (see, e.g., Klein et al. 2010 and references therein). These values are reported in Table 2; from the available data we are unable to make any significant claims about the water content of the body polluting HE 1349–2305. Comparing the measured heavy-element abundances (calcium, silicon, and magnesium) to those of well-studied polluted white dwarf stars suggests that the body polluting HE 1349–2305 has experienced radiative weathering. In particular, the accreted body exhibits the characteristic Si/Mg deficiency and Ca/Mg enhancement (relative to CI Chondrites) shown by GD 40 that

is interpreted as evidence for silicate vaporization of the parent rocky body by the intense radiation field from its evolving host star (Klein et al. 2010; Melis et al. 2011). These results suggest that HE 1349–2305 could be accreting the remnants of a differentiated rocky body, although tighter constraints on or detections of oxygen and iron are necessary before solidifying any such claim. Comparing the pollution of HE 1349–2305 to that of the other gas disk-hosting white dwarf stars (Table 2) reveals that HE 1349–2305 is among the lowest accretors of the group. Of the helium-dominated atmosphere white dwarf stars in Table 2, HE 1349–2305 has a time-averaged accretion rate that is lower than the other two (SDSS J0738 and Ton 345) by more than an order of magnitude.

The identification of a metallic gas disk orbiting HE 1349–2305 shows that there is possibly a significant population of gas disk-hosting white dwarf stars that remain to be discovered, perhaps even within the currently known population of polluted white dwarf stars.

5. CONCLUSIONS

We have observed the heavy element and hydrogen polluted white dwarf HE 1349–2305 in the optical and near-infrared. Our principal results are that the star hosts Ca II IRT emission lines indicative of orbiting gaseous debris and that there is little evidence of heavy-element pollution in its optical spectrum (compared to other disk-hosting helium-dominated atmosphere white dwarfs; Zuckerman et al. 2007; Klein et al. 2010, 2011; Dufour et al. 2012). Observations in the ultraviolet will be necessary to further examine the elemental composition of the parent body polluting this white dwarf star.

C.M. acknowledges support from the National Science Foundation under award No. AST-1003318. P.D. is a CRAQ postdoctoral fellow. This Letter includes data gathered with the 6.5 m Magellan Telescopes located at Las Campanas Observatory, Chile. This work is based partly on observations made with ESO Telescopes at Paranal Observatory under the program 087.D-0858(A). This publication makes use of data products from the Two Micron All Sky Survey, which is a joint project of the University of Massachusetts and the Infrared Processing and Analysis Center/California Institute of Technology, funded by the National Aeronautics and Space Administration and the National Science Foundation. This research has made use of the SIMBAD database and VizieR service. This work is based on observations made with the NASA *Galaxy Evolution Explorer*. GALEX is operated for NASA by the California Institute of Technology under NASA contract NAS5-98034. This work is supported in part by the NSERC Canada and by the Fund FQRNT (Québec).

Facilities: Magellan:Clay (MagE), VLT:Kueyen (X-shooter), Nickel (Direct Imaging Camera), Shane (Gemini), IRTF (SpeX)

REFERENCES

- Bessel, M. S. 1990, *A&AS*, **83**, 357
 Bessel, M. S. 1990, *PASP*, **102**, 1181
 Bochanski, J. J., Hennawi, J. F., Simcoe, R. A., et al. 2009, *PASP*, **121**, 1409
 Brinkworth, C., Gänsicke, B., Girven, J., et al. 2012, *ApJ*, **750**, 86
 Brinkworth, C. S., Gänsicke, B. T., Marsh, T. R., Hoard, D. W., & Tappert, C. 2009, *ApJ*, **696**, 1402
 Cushing, M. C., Vacca, W. D., & Rayner, J. T. 2004, *PASP*, **116**, 362
 Debes, J. H., & Sigurdsson, S. 2002, *ApJ*, **572**, 556
 D’Oroico, S., Dekker, H., Mazzoleni, R., et al. 2006, *Proc. SPIE*, **6269**, 98
 Dufour, P., Bergeron, P., & Fontaine, G. 2005, *ApJ*, **627**, 404
 Dufour, P., Bergeron, P., Liebert, J., et al. 2007, *ApJ*, **663**, 1291

- Dufour, P., Kilic, M., Fontaine, G., et al. 2010, *ApJ*, **719**, 803
- Dufour, P., Kilic, M., Fontaine, G., et al. 2012, *ApJ*, **749**, 6
- Epchtein, N., de Batz, B., Capolani, L., et al. 1997, *Messenger*, **87**, 27
- Farihi, J., Barstow, M. A., Redfield, S., Dufour, P., & Hambly, N. C. 2010a, *MNRAS*, **404**, 2123
- Farihi, J., Brinkworth, C. S., Gänsicke, B. T., et al. 2011a, *ApJ*, **728**, L8
- Farihi, J., Gänsicke, B. T., Steele, P. R., et al. 2011b, *MNRAS*, **421**, 1635
- Farihi, J., Jura, M., Lee, J., & Zuckerman, B. 2010b, *ApJ*, **714**, 1386
- Farihi, J., Jura, M., & Zuckerman, B. 2009, *ApJ*, **694**, 805
- Gänsicke, B. T., Koester, D., Marsh, T. R., Rebassa-Mansergas, A., & Southworth, J. 2008a, *MNRAS*, **391**, L103
- Gänsicke, B. T., Marsh, T. R., & Southworth, J. 2007, *MNRAS*, **380**, L35
- Gänsicke, B. T., Marsh, T. R., Southworth, J., & Rebassa-Mansergas, A. 2006, *Science*, **314**, 1908
- Gänsicke, B. T., Marsh, T. R., Southworth, J., & Rebassa-Mansergas, A. 2008b, in ASP Conf. Ser. 398, Extreme Solar Systems, ed. D. Fischer, F. A. Rasio, S. E. Thorsett, & A. Wolszczan (San Francisco, CA: ASP), 149
- Girven, J., Brinkworth, C. S., Farihi, J., et al. 2012, *ApJ*, **749**, 154
- Hamuy, M., Suntzeff, N. B., Heathcote, S. R., et al. 1994, *PASP*, **106**, 566
- Jura, M. 2003, *ApJ*, **584**, L91
- Jura, M. 2008, *AJ*, **135**, 1785
- Jura, M., & Xu, S. 2012, *AJ*, **143**, 6
- Klein, B., Jura, M., Koester, D., & Zuckerman, B. 2011, *ApJ*, **741**, 64
- Klein, B., Jura, M., Koester, D., Zuckerman, B., & Melis, C. 2010, *ApJ*, **709**, 950
- Koester, D. 2009, *A&A*, **498**, 517
- Koester, D., Rollenhagen, K., Napiwotzki, R., et al. 2005, *A&A*, **432**, 1025
- Marshall, J. L., Burles, S., Thompson, I. B., et al. 2008, *Proc. SPIE*, **7014**, 169
- Martin, D. C., Fanson, J., Schiminovich, D., et al. 2005, *ApJ*, **619**, L1
- McLean, I. S., Becklin, E. E., Brims, G., et al. 1993, *Proc. SPIE*, **1946**, 513
- Melis, C., Farihi, J., Dufour, P., et al. 2011, *ApJ*, **732**, 90
- Melis, C., Jura, M., Albert, L., Klein, B., & Zuckerman, B. 2010, *ApJ*, **722**, 1078
- Morrissey, P., Conrow, T., Barlow, T. A., et al. 2007, *ApJS*, **173**, 682
- Rayner, J. T., Toomey, D. W., Onaka, P. M., et al. 2003, *PASP*, **115**, 362
- Skrutskie, M. F., Cutri, R. M., Stiening, R., et al. 2006, *AJ*, **131**, 1163
- Vacca, W. D., Cushing, M. C., & Rayner, J. T. 2003, *PASP*, **115**, 389
- Voss, B., Koester, D., Napiwotzki, R., Christlieb, N., & Reimers, D. 2007, *A&A*, **470**, 1079
- Zuckerman, B., Koester, D., Melis, C., Hansen, B. M., & Jura, M. 2007, *ApJ*, **671**, 872
- Zuckerman, B., Melis, C., Klein, B., Koester, D., & Jura, M. 2010, *ApJ*, **722**, 725